View metadata, citation and similar papers at core.ac.uk

brought to you by CORE

provided by NASA Technical Reports Server

NASA TN D-1131

TECHNICAL NOTE

D-1131

PROJECT ECHO — HORN-REFLECTOR ANTENNA FOR SPACE COMMUNICATION

A. B. Crawford, D. C. Hogg, and
L. E. Hunt
Bell Telephone Laboratories

NATIONAL AERONAUTICS AND SPACE ADMINISTRATION
WASHINGTON
December 1961

1U

TND-1131

PROJECT ECHO — HORN-REFLECTOR ANTENNA FOR SPACE COMMUNICATION

by
A. B. Crawford, D. C. Hogg, and L. E. Hunt
Bell Telephone Laboratories

SUMMARY

This paper describes the mechanical features of the horn-reflector antenna used for receiving signals reflected from the Project Echo balloon satellite, and presents in some detail the electrical characteristics (radiation patterns and gain) measured at a frequency of 2390 Mc. Theoretically derived characteristics which agree very well with the measurements are also presented; details of the calculations are given in the appendices.

PREFACE

The Project Echo communications experiment was a joint operation by the Goddard Space Flight Center of the National Aeronautics and Space Administration (NASA), the Jet Propulsion Laboratory, (JPL), the Naval Research Laboratory (NRL), and the Bell Telephone Laboratories (BTL). The equipment described herein, although designed by BTL as part of its own research and development program, was operated in connection with Project Echo under contract NASW-110 for NASA. Overall technical management of Project Echo was the responsibility of NASA's Goddard Space Flight Center.

CONTENTS

TND-1131

PROJECT ECHO — HORN-REFLECTOR ANTENNA FOR SPACE COMMUNICATION *

by
A. B. Crawford, D. C. Hogg, and L. E. Hunt
Bell Telephone Laboratories

INTRODUCTION

The horn-reflector type of antenna was originated at the Bell Telephone Laboratories facility in Holmdel, New Jersey, in the early 1940's (Reference 1) and is now in extensive use in the Bell System's transcontinental microwave relay network (Reference 2). It is a combination of a square electromagnetic horn and a reflector that is a sector of a paraboloid of revolution (Figure 1). The apex of the horn coincides with the focus of the paraboloid. Since the antenna design is based on geometrical optics and has no frequency-sensitive elements, it is extremely broadband; it is not polarization-sensitive and can be used in any linear or circular polarization. It is essentially an offset paraboloidal antenna, so that very little of the energy incident on the reflector is reflected back into the feed to produce an impedance mismatch. Because of the shielding effect of the horn, the far side and back lobes are very small.

These features, together with high aperture efficiency, make the horn-reflector antenna attractive for use in satellite communication systems. In particular, the low side and back lobes insure that when the antenna beam is pointed to the sky very little noise power is received from the ground;† thus the antenna is a low-noise transducer which permits exploitation of the low-noise features of the maser amplifier. An effective noise temperature of about 2°K has been measured for the horn-reflector type of antenna (Reference 4).

---

*The substance of this paper was published in the Bell System Technical Journal, Vol. XL, No. 4, July 1961. It is republished, with minor revisions, by permission of Bell Telephone Laboratories.

†A discussion of the noise properties of antennas is given in Reference 3.

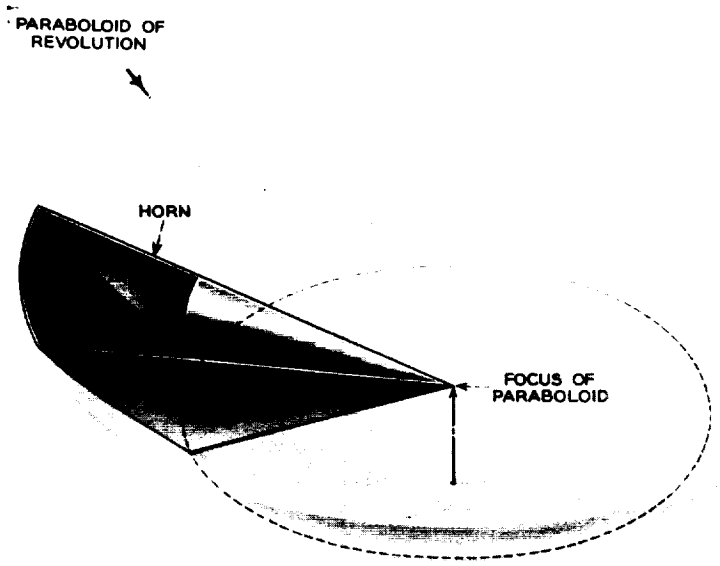

Figure 1 — Sketch showing relationship of horn-reflector antenna to a paraboloid of revolution

MECHANICAL DESCRIPTION OF THE ANTENNA

Figure 2 shows the horn-reflector antenna, erected on the Crawford Hill site of the Holmdel Laboratory, as used in the Project Echo experiment. To permit the antenna beam to be directed to any part of the sky, the antenna is mounted with the axis of the horn horizontal. Rotation about this axis affords tracking in elevation, and the entire assembly is rotated about a vertical axis for tracking in azimuth. The antenna is about 50 feet in length, the radiating aperture is approximately 20 by 20 feet, and the weight is about 18 tons. The structure was designed to survive winds of 100 miles per hour.

The elevation structure, both horn and reflector, is constructed of aluminum. The elevation wheel, 30 feet in diameter, supports all radial loads and rotates on rollers mounted on the base frame. All axial or thrust loads are taken by a large ball bearing at the apex end of the horn. The horn proper continues through this bearing into the equipment cab. Here is located a tapered (from square to round waveguide) transition section, a rotating joint, and waveguide take-offs which provide for the simultaneous reception of either two orthogonal linearly polarized signals or two circularly polarized signals of opposite sense. The ability to locate the receiver equipment at the apex of the horn, thus eliminating the loss and noise contribution of a connecting line, is an important feature of this antenna.

The triangular base frame is constructed of structural steel shapes. It rotates on wheels about a center pintle ball bearing on a track 30 feet in diameter. The track

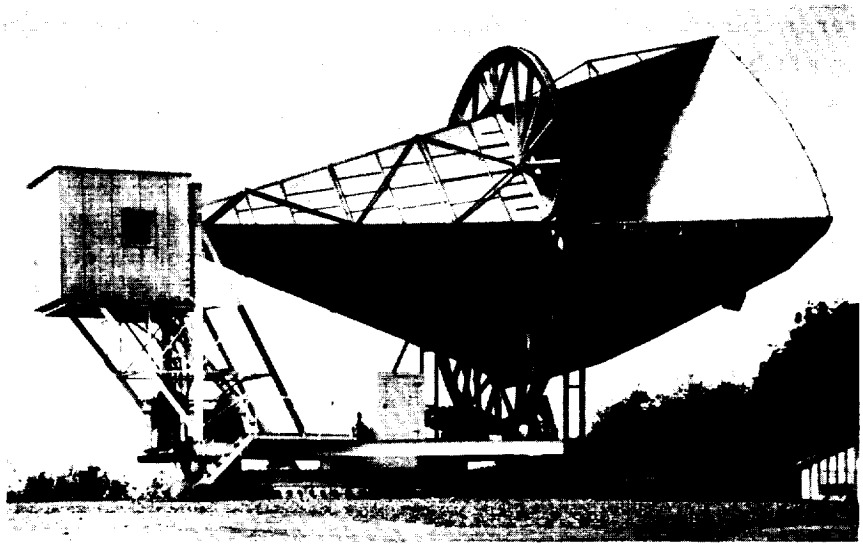

Figure 2 — Horn-reflector antenna used in Project Echo experiment

consists of stress-relieved planed steel plates which were individually adjusted to produce a track which was flat to within approximately 1/64 inch. The faces of the wheels are cone-shaped to minimize sliding friction. A tangential force of about 100 pounds is sufficient to start the antenna in motion.

The horn flares at an angle of 28 degrees. As can be seen in Figure 1, the antenna is generated by swinging the side projection through this angle. Thus the two sides of the horn are flat surfaces and the front and back surfaces are conic sections. There are several advantages to this type of construction: right-angle sections can be used for the corners of the horn; the reflector can be constructed of identical longitudinal sections; the intersections of the front and back conical surfaces with the paraboloid of revolution are circles in planes perpendicular to the axis of the paraboloid, thus providing accurate and readily available references for use in constructing the reflector. Nine accurately fabricated parabolic ribs were used for the reflector; one end of each was fastened to a curved (arc of a circle) beam at the wheel and the other end was fixed on a circle scribed on a temporary horizontal work table. The ribs were tied together by cross bracing and by a large triangular crossbeam, which in turn was tied by columns to the vertical wheel. The aluminum sheets that make up the reflecting surface were then fastened to the ribs; these have curved stiffeners to produce the small curvature required in the plane perpendicular to the ribs. It is believed that the reflector surface is accurately paraboloidal to $\pm$ 1/32 inch.

The antenna is driven in azimuth and elevation by 10 hp direct-current servo gearmotors.* Power is transmitted by sprockets (with teeth specially cut for rack operation) to roller chains which are fastened to the vertical wheel and to the plates forming the horizontal track. The roller chain proved to be a satisfactory substitute for a large bull gear; by the use of a radial arm and dial indicator, the rollers of the chains were adjusted to lie on 30-foot-diameter circles to an accuracy of about 0.005 inch. The maximum speed of rotation in both azimuth and elevation is 5 degrees per second; the maximum angular acceleration for both axes is 5 degrees/second^2. Power for the drives is brought to the rotating structure through a slip-ring assembly inside the small plywood house located over the center bearing (Figure 2). All the electrical circuits needed for the operation of the antenna and the receiving equipment in the cab come through the slip-ring assembly.

Positional information for the antenna is derived from data units driven by large (48-inch) accurately cut and accurately aligned gears located on the bearings at the apex of the horn and at the center of the base frame. The data units contain synchro transmitters and control transformers operated in a two-speed, 1:1 and 36:1, system.

The antenna has performed well electrically and mechanically during the Project Echo experiment. It has been customary to disengage the azimuth sprocket drive when the antenna is not in use, thus permitting the structure to "weathervane" and seek a position of minimum wind resistance. The structure was subjected to winds of 80 mph during Hurricane Donna, September 12, 1960, without damage.

THEORETICAL DISCUSSION

The manner in which the spherical wave diverges from the apex of the horn is shown schematically in Figure 3(a). The wave, for the greater part, maintains the characteristic amplitude distribution of the TE_{10} mode as it proceeds along the horn; nevertheless, it is a spherical wave and undergoes inverse distance attenuation up to the point where it is rendered equiphase by the paraboloidal reflector. Thus, over the surface of the projected aperture, s in Figure 3(a), the field has an unsymmetrical amplitude taper in the direction of the horn axis due to inverse distance attenuation, in addition to the symmetrical characteristic of the TE_{10} mode.

In Figure 3(b), two sets of vectors, t and ℓ, representing transverse and longitudinal polarization in the projected aperture, are shown. On the bisector of the aperture, t is parallel to the x-axis and ℓ to the y-axis; however, at points removed from the bisector,

*This is more power than is required, particularly for the elevation drive, but these motor and control packages were readily available standard items.

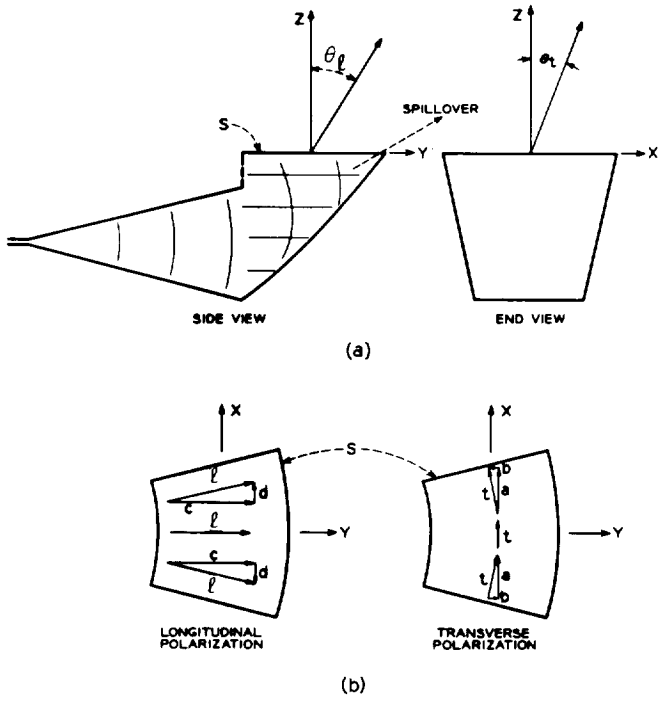

Figure 3 — Sectional views in the longitudinal (y-z) and transverse (x-z) planes and field components in the projected aperture

t and ℓ preserve the polarization established in the pyramidal horn, and therefore are inclined with respect to the principal axes. At these points, t and ℓ are broken down into components a, b and c, d respectively. Note that there is asymmetry about the bisector in the cross components b and d.

The aperture field being known, the field at a large distance R in the region near the axis of the beam can be calculated to a good approximation by

$$\mathbf{E} = \frac{j}{\lambda R} \int_S \mathbf{E}_i \exp\left[-j\beta(y \sin\theta_\ell + x \sin\theta_t)\right] ds , \qquad (1)$$

where $\mathbf{E}_i$ represents any one of the components a, b, c, or d, and θ_ℓ and θ_t are angles in the principal plane, which either contains or is transverse to the axis of the pyramidal horn. The longitudinal plane contains the horn and beam axes; the transverse plane contains the beam axis and is normal to the axis of the horn. Thus, in Figure 3, θ_ℓ lies in the yz plane and θ_t in the xz plane. Both the principal and cross-polarized radiation patterns* may be computed by using Equation 1, provided the appropriate aperture field component $\mathbf{E}_i$ is chosen. The computed patterns are shown in Figures 4, 5, and 6 as

*Details are given in Appendix A.

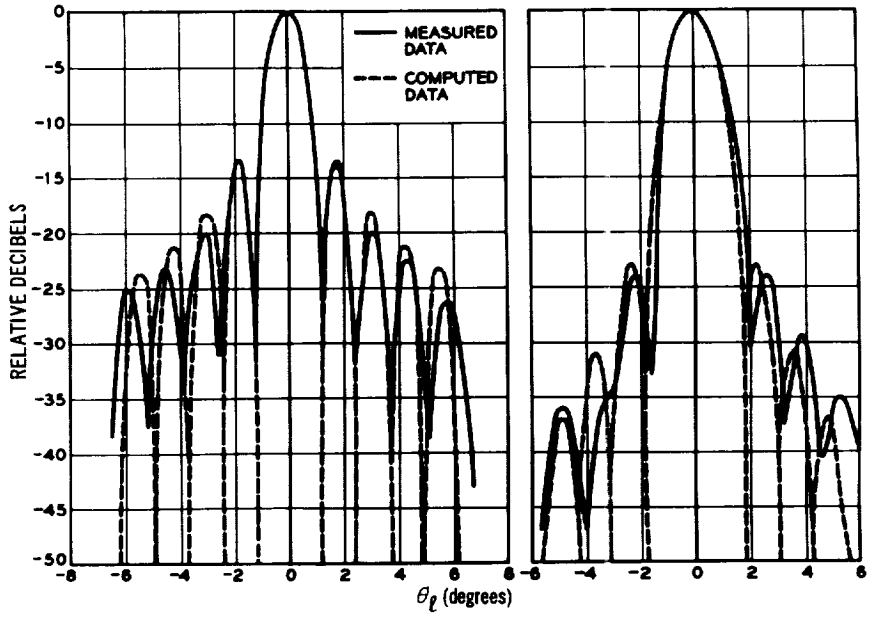

Figure 4 — Principal radiation patterns in the longitudinal plane (2390 Mc)

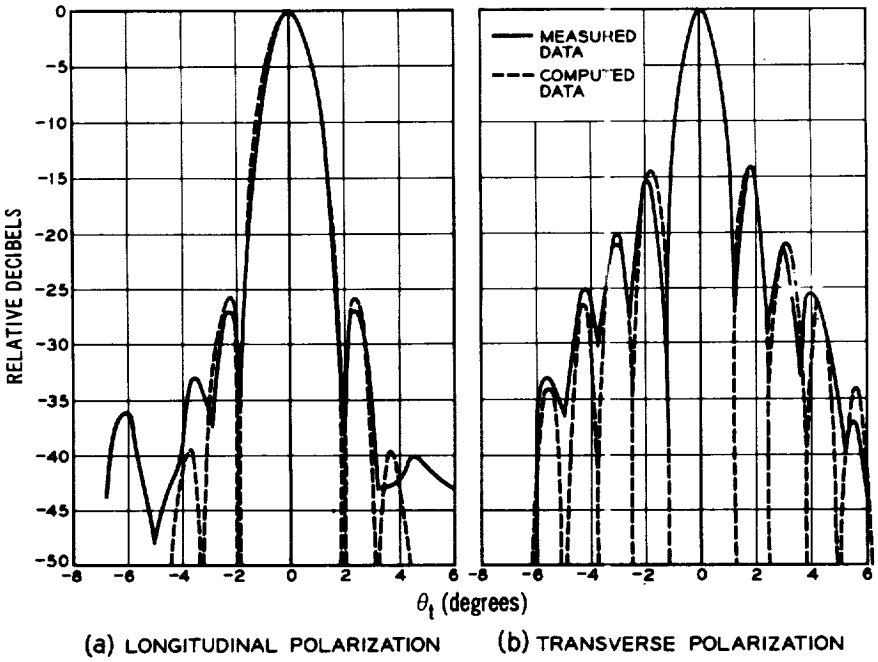

Figure 5 — Principal radiation patterns in the transverse plane (2390 Mc)

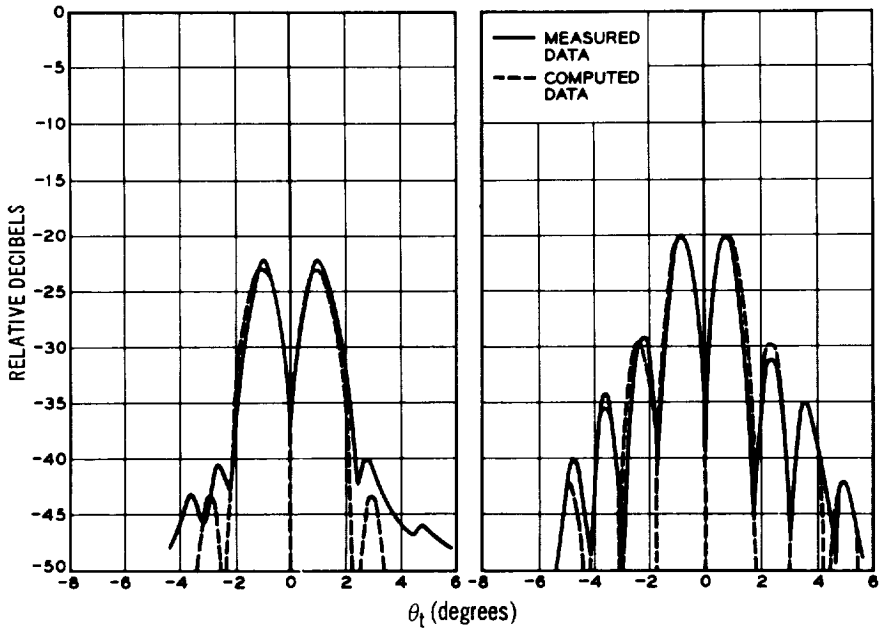

Figure 6 — Cross-polarized radiation patterns in the transverse plane (2390 Mc)

dashed curves*; the experimental data are shown as solid lines and will be discussed later. The two cross-polarization patterns in the longitudinal plane are zero for all angles because the aperture field components b and d are antisymmetrical with respect to that plane.

The radiation patterns for circular polarization may be calculated by combining the appropriate principal and cross-polarized components of the far field. An example of the method used is given in Appendix B. The dashed lines of Figures 7(a) and 8(a) show calculated radiation patterns where the antenna receives the desired (transmitted) sense of circular polarization, and Figures 7(b) and 8(b) show the undesired sense. Note especially Figures 8(a) and (b) for the transverse plane, in which the patterns are unsymmetrical with respect to the $\theta_t = 0$ axis; in Figure 8(a), the maximum of the main beam is at $\theta_t = 0.1$ degree. This effect is more clearly demonstrated by assuming that the antenna receives both clockwise and counter-clockwise senses simultaneously, as would be the case for a linearly polarized incident wave; the beam, for one sense, shifts to $\theta_t = 0.1$ degree and for the other to $\theta_t = -0.1$ degree; this effect is shown in Figure 9. The slight tilting of the beam in circular polarization is a consequence of asymmetry in the phase of the cross-polarized components of the far field.

*The computations were made for points separated by 0.25 degree in θ; thus, although the dashed curves extend to the -50 db level, they do not represent the depths of the nulls for the case of longitudinal plane patterns, but rather only their positions.

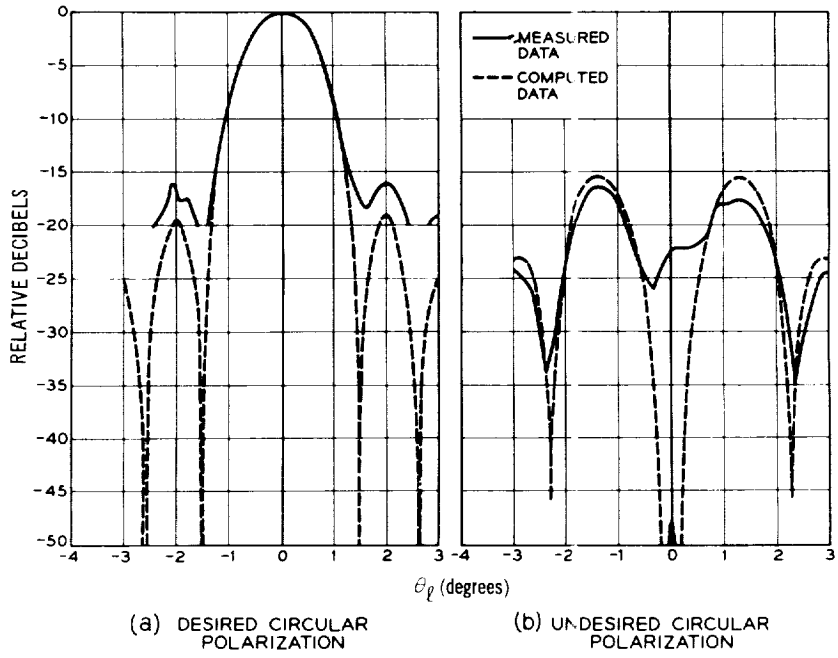

Figure 7 – Circularly polarized radiation pattern in the longitudinal plane (2390 Mc)

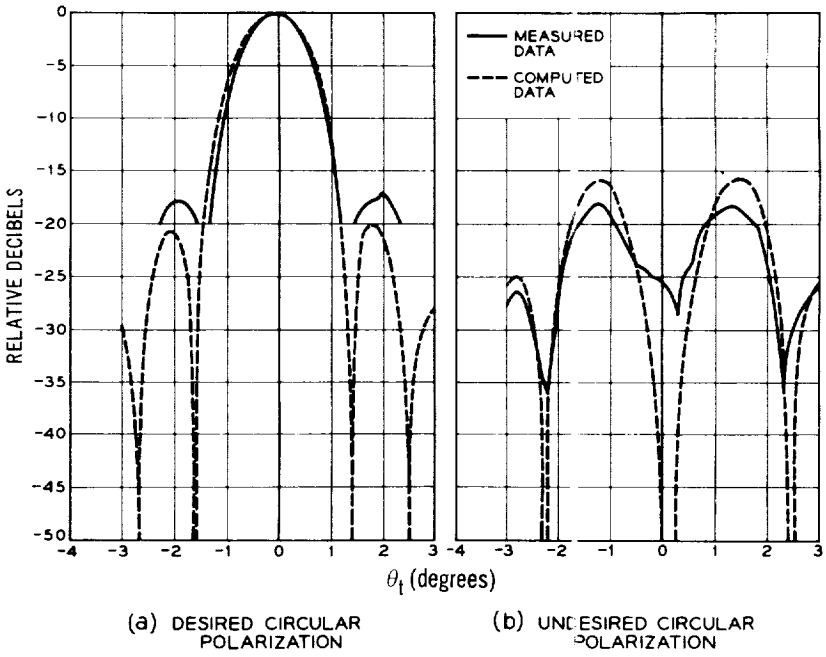

Figure 8 – Circularly polarized radiation patterns in the transverse plane (2390 Mc)

Unfortunately, all the energy which proceeds along the horn does not illuminate the paraboloidal reflecting surface; some of it is diffracted at the edge of the horn aperture. As is indicated by the dashed line in Figure 3(a), the wave is again diffracted by the edge of the reflector and produces perturbations in the far-field pattern. The lobes thus produced are referred to as spillover lobes; in Appendix D a method of calculating them is discussed. The points in Figure 10 show the spillover effect calculated for longitudinal polarization in the longitudinal plane. The maximum spillover energy is at an angle $\theta \approx 70$ degrees; as is indicated in the insert in Figure 11, this differs by 7 degrees from the direction determined by the flare angle of the horn, namely, 77 degrees. For transverse polarization, the spillover effect is much reduced because of the cosine distribution in the z direction in the horn for that polarization.

TECHNIQUE OF MEASUREMENTS

The important electrical properties of the antenna to be measured are its gain and radiation patterns at the frequency of interest, in this case 2390 Mc. To make such measurements, it is necessary to provide a known incident field. In free space, ideally, the incident field would be uniform in amplitude and phase over the region occupied by the aperture of the antenna. In practice, this is accomplished by placing a source at such a distance that the wave incident at the antenna under test is essentially plane. The usual criterion is that the phase deviation over the aperture not exceed $\pi/8$. For the 20-foot aperture considered here, this criterion requires that a test transmitter operating at 2390 Mc be at least one-third mile away; the distance used for these tests was about two miles. The antenna is not in free space, however, and environment such as trees and contours of the local terrain introduce reflections which distort the incident field. For these tests, nearby trees were removed and, both before and after the antenna was in place, the incident field was checked by exploring it with a probe consisting of a small horn. This horn was mounted on a motor-driven carriage that was drawn up and down a 55-foot vertical tower, the received output being continuously recorded. The tower was set at several horizontal positions, so the incident field over the area to be occupied by the antenna was mapped out. These height runs showed irregular variations in the incident field, but these did not exceed ±1 db, and therefore were considered small enough to permit meaningful measurements. An analysis of the height runs indicated that, in addition to the direct space wave, a second wave, reflected from the intervening ground, was also present. The analysis fixed the reflection point at about midpath at an elevation corresponding to the tree-top level, with an amplitude reflection coefficient of about 0.07.

GAIN MEASUREMENTS

The gain of the horn-reflector antenna was measured by comparing the strength of its received signal with that of a standard horn.* The latter was located in the plane of the

*This was a pyramidal horn whose gain at 2390 Mc, calculated from its physical dimensions, was 20.1 db.

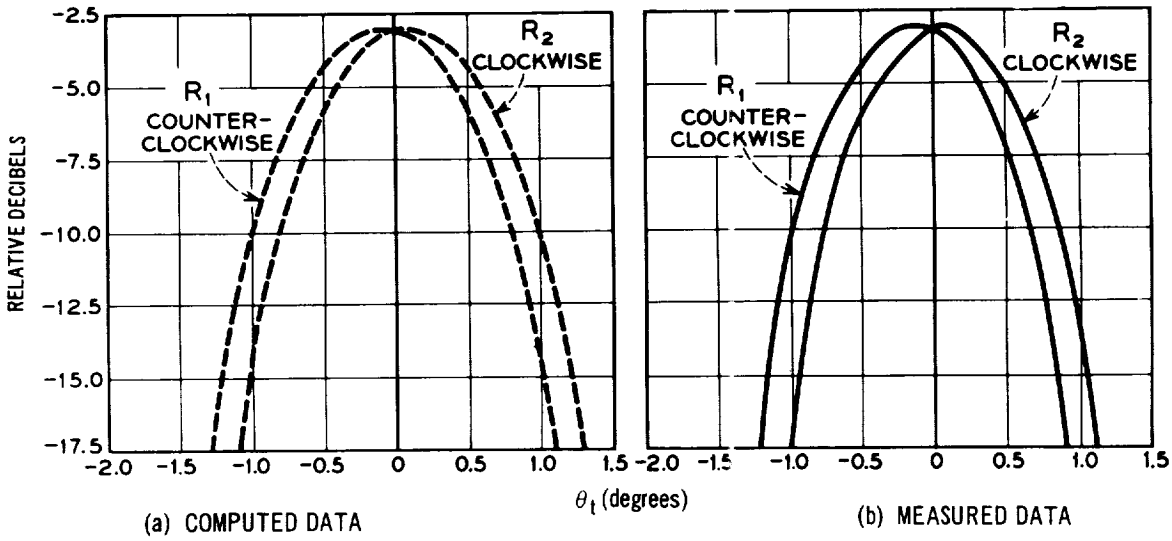

Figure 9 — Circularly polarized radiation patterns in the transverse plane, showing dependence of beam displacement on sense of polarization

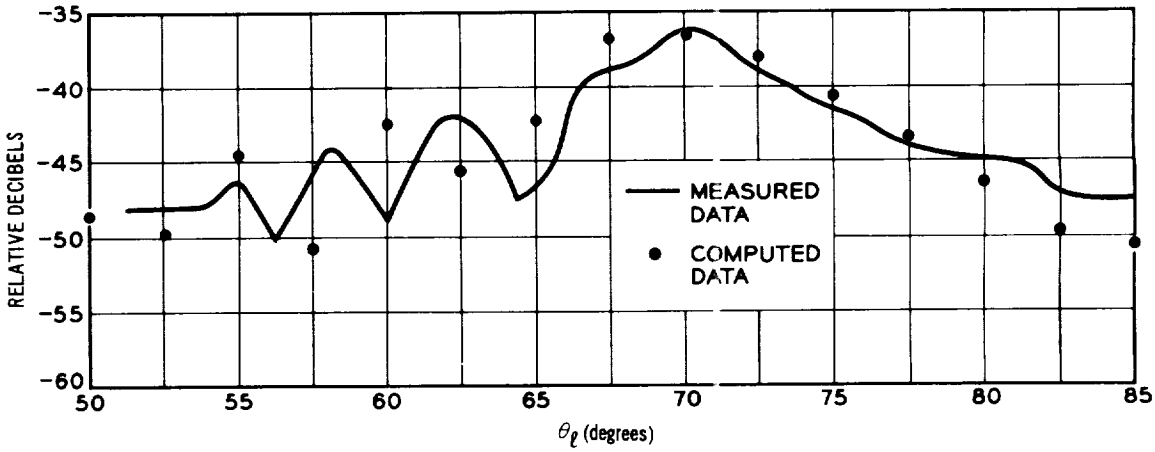

Figure 10 — Calculated and measured spillover lobe; longitudinal plane, longitudinal polarization

aperture of the horn-reflector, but off to one side. The field at this particular location of the standard horn was equal to the average intensity of the field illuminated the horn reflector, as obtained from the height run data.

The measurement procedure consisted first of aiming the horn-reflector for optimum received signal strength and continuously recording the output. Because of scintillation of the signal, it was necessary to integrate for several seconds to obtain a dependable signal level. The coaxial line which fed the receiver was then shifted from the horn-reflector to the standard horn and the results were recorded for a like period. A number of such comparisons were made. The gain of the horn-reflector, referred to an isotropic radiator, was then obtained by adding the db difference between those two signal strengths to the db gain of the standard horn.

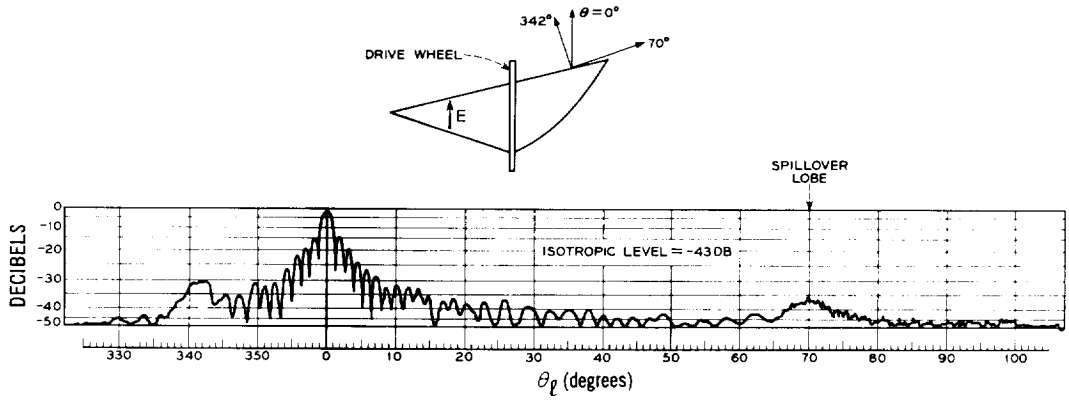

Figure 11 — Extended radiation pattern; longitudinal plane, longitudinal polarization

A double detection receiver was used in all the measurements. Signal-level differences were established by an attenuator in the intermediate frequency (65 Mc) channel which was calibrated to an accuracy of ±0.05 db. The gain was measured using both longitudinal and transverse polarizations and the results were averaged:

1. The calculated gain of the standard horn was 20.1 db;
2. The measured gain of the horn-reflector over the standard horn was 23.2 db;
3. The gain of the horn-reflector was 43.3 db.

The rms scatter of the gain measurements was 0.16 db, owing principally to scintillation of the signal.

The theoretical value for the horn-reflector gain is calculated by the method discussed in Appendix C. Because of the asymmetrical geometry of the aperture, the gain depends slightly on polarization, being 43.43 db for longitudinal and 43.35 db for transverse. The average theoretical gain is therefore 43.39 db; this is 1.12 db below the actual full area gain (44.51 db).

If we compare the measured and calculated values, the gain is 0.09 db less than expected.* Part of this discrepancy is due to the irregularities in the incident field discussed above in connection with the height run data. If it is assumed that the variations in the phase of the incident field are random over the aperture (the deviation of the phase variation being derived from the 0.07 db reflection coefficient discussed above) the decrease in received signal † due to this effect can be estimated. This turns out to be 0.02 db, so that the discrepancy between calculated and measured values is reduced slightly. The remainder is most likely due to spillover.

PATTERN MEASUREMENTS

Radiation patterns were obtained by continuously recording the receiver output as the horn-reflector was rotated at a constant speed. There are several directional patterns of

*In other words, the measured effective area is 1.2 db below actual area, or the measured efficiency is 76 percent.

† For a small random fluctuation, the decrease in signal is $e^{-\delta^2}$ where δ is the standard deviation of the fluctuations in phase (Reference 5).

interest; these include the principal and cross-polarized patterns for the linear polarizations in the two principal planes, and patterns in circular polarization for the two planes. As was discussed in an earlier section, the two cross-polarized patterns in the longitudinal plane are expected to be zero, because of the odd symmetry of the cross-polarized components of the aperture field.

Detailed patterns for the principal polarizations in the region of the main beam are shown in Figures 4 and 5 for longitudinal and transverse planes respectively. In general, the measurements agree very well with the calculated patterns except for some relatively small departures considered to be due to reflections from the environment and to scintillation. The salient factors obtained from the principal linear polarization patterns are shown in Table 1.

Table 1

Significant Factors of Linear Polarization Patterns

Plane	Polarization	3-db Beamwidths (degrees)		Level of First Minor Lobes (db)	
		Measured	Calculated	Measured	Calculated
transverse	longitudinal	1.35	1.30	-27	-26.5
longitudinal	longitudinal	1.10	1.10	-13.5	-13.5
transverse	transverse	1.00	1.00	-14.5	-14.5
longitudinal	transverse	1.55	1.55	-24.0	-23.0

The cross-polarization patterns in the transverse plane are shown in Figure 6; here also the agreement between experiment and theory is considered to be good. The levels of cross-polarization in the longitudinal plane, which are theoretically zero, were lower than -30 db in the region near $\theta_\ell = 0$ and fell rapidly to less than -45 db for other angles.

The response of the antenna to circularly polarized waves is shown by the patterns of Figures 7 through 9. In general, the agreement between measurement and theory is not as satisfactory as for the linear polarization patterns; this disagreement is believed due in part to lack of sufficient measuring range in the receivers used for the two circular senses. When both the transmitting test antenna and the horn-reflector were adjusted for the same sense of polarization, the first side lobes in both the longitudinal and transverse planes, as seen in Figures 7(a) and 8(a), measured about 3 db higher than the values predicted by theory; the main beamwidths, however, agreed well with calculations. When the horn-reflector was adjusted to receive the sense opposite to that transmitted, the response on the first side lobes, as shown in Figures 7(b) and 8(b), was about 2 db lower than that predicted, and the response in the direction of the principal axis was about -27 db. The discrepancy between this value and that predicted by theory is believed due

partly to depolarization by the ground and partly to imperfect circular polarization from the transmitter.*

A test was made in which the horn-reflector received, simultaneously, both senses of circular polarization generated by a linearly polarized wave from the test transmitter. The results appear in Figure 9; the slight beam tilt, as evidenced by the displacement in opposite directions from $\theta_t = 0$, depending on the sense of polarization, agrees well with theoretical values. A similar displacement between the two senses was observed while receiving noise from the moon and sun.

Figure 11 shows an extended radiation pattern measured in the longitudinal plane with longitudinal polarization. Let us refer to this region as the spillover sector; it is shown here in preference to any other sector because the level of the far-side lobes is of the order of the isotropic level rather than 10 to 30 db or so below isotropic, as is the case for the other sectors (References 2 and 4). The most prominent spurious lobe is the so-called spillover lobe at an angle of 70 degrees from the main beam. A more detailed plot of the spillover lobe is shown in Figure 10, the points being values calculated in Appendix D. The agreement in level and shape of the measured curve and calculated points is fairly good; however, the calculated data appear to be translated about two degrees toward smaller values of θ_ℓ. Pattern measurements with transverse polarization showed much lower levels for the far lobes in the spillover sector.

Also apparent in Figure 11 is a prominent lobe at an angle of 342 degrees. This lobe is apparently associated with the 30-foot-diameter drive wheel which, as may be seen in the insert in Figure 11, tends to shadow the aperture in that direction. Diffraction over the rim of the wheel might cause this spurious lobe.

CONCLUDING REMARKS

The performance characteristics of this relatively large horn-reflector type of antenna, measured at a frequency of 2390 Mc, agree satisfactorily with its calculated performance. The measured radiation patterns are readily identified with those calculated to at least the third side lobes, the antenna gain being about one-tenth decibel less than was expected. This good performance, in conjunction with the low-noise properties of this type of antenna, make it favorable not only for use in space communications, but also for use as a standard for absolute flux measurements in radio astronomy. Of some concern is a small amount of spillover which degrades the performance in one sector of

*The circular polarization was produced by a quarter-wave plate placed in front of the transmitting horn; the axial ratio, measured by rotating a 20-db horn antenna at the receiving site, was about 0.8 db.

the radiation pattern; fortunately, in the above applications, the spillover sector is directed skyward and therefore the noise contribution is small in the microwave band.

ACKNOWLEDGMENTS

With the exception of the steel base frame, which was fabricated by a local steel company, the antenna was constructed and assembled by the Holmdel Laboratory shops under the direction of H. W. Anderson, who also collaborated in the design. Assistance in the design was also given by R. O'Regan, S. A. Darby and several members of the electro-mechanical development group at the Whippany Laboratory. The latter group also was instrumental in procuring special equipment, such as data units, gears, and slip-ring assembly.

Assistance in the assembly and adjustment of electrical components and in the measurement of the electrical properties of the antenna was given by R. A. Semplak, H. A. Gorenflo, and R. A. Desmond. Computation of the theoretical data was made by Mrs. C. L. Beattie.

REFERENCES

1. Friis, H. T., and Beck, A. C., "Directional Antenna," U. S. Patent 2,236,393, March 1, 1941

2. Friis, R. W., and May, A. S., "A New Broad-Band Microwave Antenna System" A.I.E.E. Trans., Pt. I, 77:97-100, 1958

3. Hogg, D. C., "Problems in Low Noise Reception of Microwaves," I.R.E. Trans., Propagation Section 8.2, Nat. Symp. on Space Electronics and Telemetry, 1960.

4. DeGrasse, R. W., Hogg, D. C., Ohm, E. A., and Scovil, H.E.D., "Ultra-Low-Noise Antenna and Receiver Combination for Satellite or Space Communication," Proc. Nat. Elect. Conf. 15:370-379, 1959

5. Ruze, J., "The Effect of Aperture Errors on the Antenna Radiation Pattern," Nuovo Cimento 9 (suppl. 3):364-380, 1952

6. Woonton, G. A., "The Effect of an Obstacle in the Fresnel Field on the Distant Field of a Linear Radiator," J. Appl. Phys. 21:577-580, June 1950

Appendix A

Calculation of Patterns for Linear Polarization

The radiation patterns for linear polarization in the region of the main beam of the antenna are calculated from:

$$E = \frac{j}{\lambda R} \int_S E_i \exp\left[-j\beta(y \sin\theta_\ell + x \sin\theta_t)\right] ds, \qquad \text{(A1)}$$

where E_i is a component of the aperture field and x, y are coordinates in the projected aperture, S; R is the distance from the antenna to the distant field point; θ_ℓ and θ_t are angles in the principal planes; $\beta = 2\pi/\lambda$.

Since energy proceeds down the square horn in essentially a dominant waveguide mode, the field is constant along one coordinate and has a cosine distribution along the orthogonal coordinate. In addition, the field of the spherical wave decreases inversely with the distance ρ shown in Figure A1(a); but, since the spherical phase front is corrected by the reflector, only negligible attenuation occurs between the reflector and the projected aperture, S, in the plane AA'.

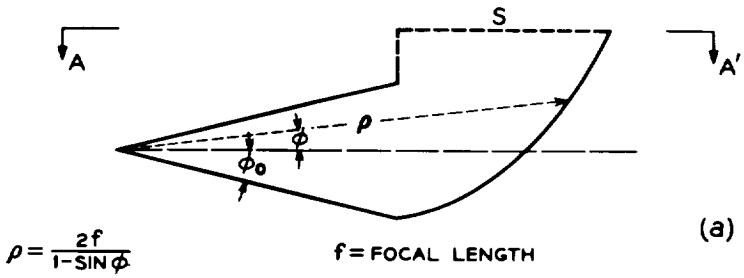

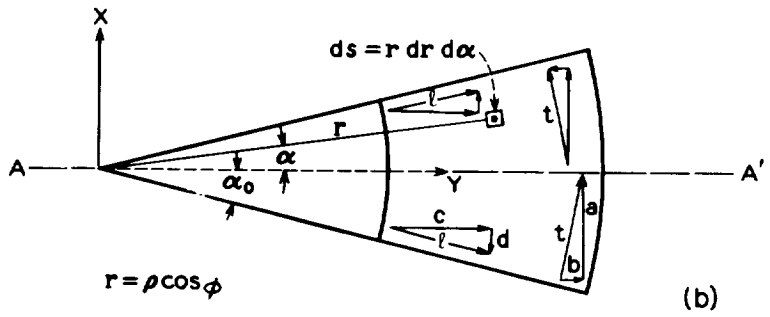

Figure A1 — Coordinate system and projected aperture,

The total fields ℓ and t, and the field components a, b, c, and d in the projected aperture, are shown in Figure A1(b). Each of these can be expressed in terms of the symbols shown in the figure:

$$\left.\begin{aligned} E_a &= E_0 \frac{\rho_0}{\rho} \cos \frac{\pi\phi}{2\phi_0} \cos \alpha, \\ E_b &= E_0 \frac{\rho_0}{\rho} \cos \frac{\pi\phi}{2\phi_0} \sin \alpha, \\ E_c &= E_0 \frac{\rho_0}{\rho} \cos \frac{\pi\alpha}{2\alpha_0} \cos \alpha, \\ E_d &= E_0 \frac{\rho_0}{\rho} \cos \frac{\pi\alpha}{2\alpha_0} \sin \alpha. \end{aligned}\right\} \qquad \text{(A2)}$$

The field has been normalized to the value E_0 at $\rho = \rho_0 = 2f$ (where $\phi = \alpha = 0$), ϕ_0 and α_0 being the flare angles of the horn. Equation A2, substituted for E_i in Equation A1, results in the far-field equations. However, for comparison with experimental data, the principal plane of interest as well as the polarization must be specified; therefore let us designate the far fields as in Table A1.

Table A1

Far Field Designations

Polarization of Antenna	Plane of Measurement	Polarization of Far Field	Designation of Far Field
longitudinal	longitudinal	longitudinal	E_1
transverse	longitudinal	transverse	E_2
longitudinal	transverse	longitudinal	E_3
transverse	transverse	transverse	E_4
longitudinal	longitudinal	transverse	E_5
transverse	longitudinal	longitudinal	E_6
longitudinal	transverse	transverse	E_7
transverse	transverse	longitudinal	E_8

These designations are related to Equations A1 and A2 as follows:

$$\begin{bmatrix} E_1 \\ E_2 \\ E_5 \\ E_6 \end{bmatrix} = j \frac{4f^2}{\lambda R} \int_{-\alpha_0}^{\alpha_0} d\alpha \int_{-\phi_0}^{\phi_0} d\phi \begin{bmatrix} E_c \\ E_a \\ E_d \\ E_b \end{bmatrix} \frac{\rho}{\rho_0} \frac{\cos \phi}{1 - \sin \phi} \exp(-j\beta\rho \cos \phi \cos \alpha \sin \theta_\ell), \qquad \text{(A3)}$$

$$\begin{bmatrix} E_3 \\ E_4 \\ E_7 \\ E_8 \end{bmatrix} = j \frac{4f^2}{\lambda R} \int_{-\alpha_0}^{\alpha_0} d\alpha \int_{-\phi_0}^{\phi_0} d\phi \begin{bmatrix} E_c \\ E_a \\ E_d \\ E_b \end{bmatrix} \frac{\rho}{\rho_0} \frac{\cos \phi}{1 - \sin \phi} \exp(-j\beta\rho \cos \phi \sin \alpha \sin \theta_t). \quad \text{(A4)}$$

Integration shows that E_5 and E_6 are zero. The remainder are computed by numerical integration, with E_1, E_2, E_3, E_4, E_7, and E_8 corresponding to the patterns in Figures 4(a), 4(b), 5(a), 5(b), 6(a), and 6(b), respectively, in the body of this report.

Appendix C

Gain

The antenna gain may be calculated using

$$G = 4\pi R^2 \frac{F(0)}{P_s} , \tag{C1}$$

where $F(0) = (1/\eta) \mid E(0) \mid^2$ is the density of power flow in the direction $\theta_t = \theta_\ell = 0$ as obtained from Equation A1 of Appendix A by numerical integration ($\eta = 120\pi$); P_s, the total power radiated by the aperture, is obtained by integration of either of the components ℓ or t of Figure A1. For example, since

$$E_\ell = E_0 \frac{\rho_0}{\rho} \cos \frac{\pi\phi}{2\phi_0} \tag{C2}$$

and

$$ds = r\, dr\, d\theta = 4f^2 \frac{\cos \phi}{(1 - \sin \phi)^2} d\phi\, d\alpha , \tag{C3}$$

$$P_s = \frac{E_0^2}{\eta} 4f^2 \int_{-\alpha_0}^{\alpha_0} d\alpha \int_{-\phi_0}^{\phi_0} d\phi \cos^2 \frac{\pi\alpha}{2\alpha_0} \cos \phi = \frac{E_0^2}{\eta} 8f^2\alpha_0 \sin \phi_0 . \tag{C4}$$

The efficiency of the antenna is given by A_e/S, where $A_e = \lambda^2 G/4\pi$ is the effective area, and

$$S = \int_S r\, dr\, d\alpha = 16f^2\alpha_0 \frac{\sin \phi_0}{\cos^2 \phi_0} \tag{C5}$$

is the actual area of the projected aperture.

Appendix D

The Spillover Lobe

The spherical wave in the horn (shown in figure D1) is diffracted at edge A and part of the energy proceeds beyond the rim of the reflector, C. For the purpose of calculating the spillover lobe, the antenna configuration is idealized by replacing the curved reflector (dashed curve in Figure D1) with a plane semi-infinite sheet, the edge of which

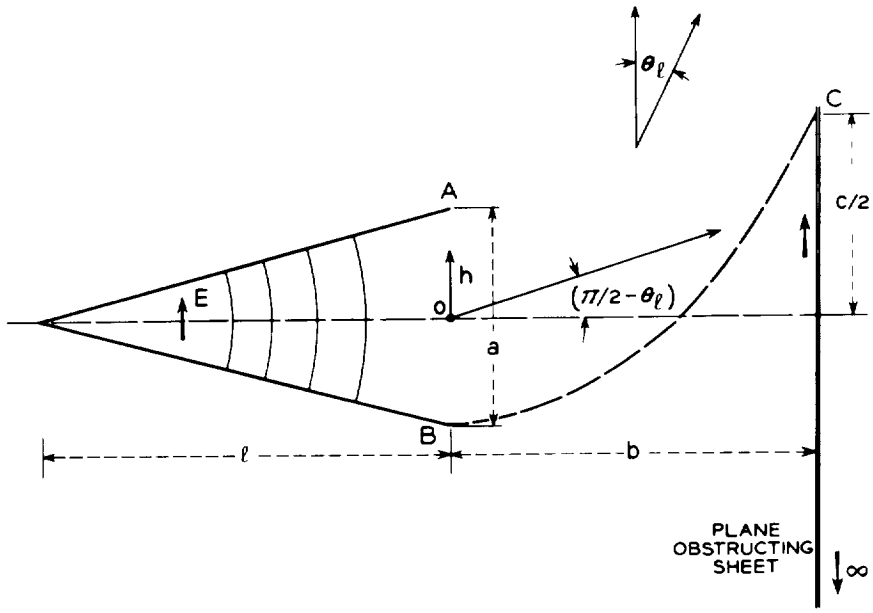

Figure D1 — Two-dimensional geometry used for calculating the spillover lobe

is c/2 above the axis of the horn. The distant field of this horn-sheet combination can then be calculated by use of Fourier transforms, as discussed by Woonton.* If discussion is restricted to the plane of Figure D1, for the distant field at a point R (θ not too far removed from the axis of the horn):

$$E' = \left(\frac{j}{2\pi\lambda R}\right)^{\frac{1}{2}} E_0 e^{j(\pi-1)\gamma^2 b\lambda} \left\{\sqrt{\lambda\ell}\; e^{j\pi\gamma^2\lambda\ell}\left[C(v_2) - C(v_1) - jS(v_2) + jS(v_1)\right] - (1+j)\sqrt{\pi}\int_{-a/2}^{a/2} e^{-j\pi(h^2/\lambda\ell - 2\gamma h)}\left[C(v_0) - jS(v_0)\right] dh\right\}, \tag{D1}$$

*Woonton, G. A., "The Effect of an Obstacle in the Fresnel Field on the Distant Field of a Linear Radiator," J. Appl. Phys. 21:577-580, June 1950

where E_0 is the field at the center of the horn aperture,

$$v_0 = \frac{1}{\sqrt{2b\lambda}} \left[c - 2(h - \gamma b\lambda) \right] ; \tag{D2}$$

$$v_1 = \sqrt{\frac{2}{\ell\lambda}} \left[\gamma\ell\lambda - a/2 \right] ; \tag{D3}$$

$$v_2 = \sqrt{\frac{2}{\ell\lambda}} \left[\gamma\ell\lambda + a/2 \right] ; \tag{D4}$$

and

$$\gamma = -(1/\lambda) \sin (\pi/2 - \theta) ; \tag{D5}$$

a is the width of the horn aperture along the h coordinate; b, c, and ℓ are the dimensions shown in Figure D1, and C and S are Fresnel integrals, respectively.

The two-dimensional solution (Equation D1) predicts quite accurately the value of θ_ℓ at which maximum spillover occurs, but it is in error in absolute value because in reality the diffracting edges A and C are of finite length and are curved. The curvature of edge C can be approximately accounted for by assuming that the diffraction effect in the plane of Figure D1 and the effect in the plane AC, normal to the figure, are separable. In that case, Equation D1 is multiplied by a factor

$$K = \frac{\int_{-d}^{d} e^{-j\pi(x^2/\lambda r)} \cos \frac{\pi x}{2d} \, dx}{\int_{-d}^{d} \cos \frac{\pi x}{2d} \, dx} , \tag{D6}$$

where x is the coordinate normal to the plane of Figure D1 at C, 2d the extent of the edge along the x-axis, and r its radius of curvature.

The values plotted in Figure C1 are KE'; K amounts to -10.5 db for the case under consideration.